

OPEN ACCESS

EDITED BY Fabio M. Squina, University of Sorocaba, Brazil

REVIEWED BY
Pengfei Zhou,
Guangdong Medical University, China
Ashish Verma,
Institute of Medical Sciences, India

*CORRESPONDENCE
Qihai Gong

☑ gqh@zmu.edu.cn

†These authors share first authorship

RECEIVED 02 July 2025 ACCEPTED 17 October 2025 PUBLISHED 07 November 2025

CITATION

Jain A, Sarsaiya S and Gong Q (2025) Cinnabar-induced hormesis in *Trichoderma longibrachiatum* MD33: multi-omics elucidation of a fungal-specific dendrobine biosynthesis pathway. *Front. Microbiol.* 16:1657982. doi: 10.3389/fmicb.2025.1657982

COPYRIGHT

© 2025 Jain, Sarsaiya and Gong. This is an open-access article distributed under the terms of the Creative Commons Attribution License (CC BY). The use, distribution or reproduction in other forums is permitted, provided the original author(s) and the copyright owner(s) are credited and that the original publication in this journal is cited, in accordance with accepted academic practice. No use, distribution or reproduction is permitted which does not comply with these terms.

Cinnabar-induced hormesis in *Trichoderma longibrachiatum* MD33: multi-omics elucidation of a fungal-specific dendrobine biosynthesis pathway

Archana Jain^{1†}, Surendra Sarsaiya^{1,2†} and Qihai Gong^{1*}

¹Key Laboratory of Basic Pharmacology and Joint International Research Laboratory of Ethnomedicine of Ministry of Education, Zunyi Medical University, Zunyi, China, ²Bioresource Institute for Healthy Utilization, Zunyi Medical University, Zunyi, China

Introduction: The endangered orchid *Dendrobium nobile* is the primary source of dendrobine, a neuroprotective sesquiterpene alkaloid, but unsustainable harvesting necessitates alternative production platforms, such as the endophytic fungus *Trichoderma longibrachiatum* MD33. However, the fungal dendrobine pathway and its regulatory mechanisms remain uncharacterized, limiting its biotechnological exploitation.

Methods: This study investigated cinnabar (HgS)-induced hormesis to elucidate the stress-mediated metabolic reprogramming of dendrobine biosynthesis through integrated transcriptomic and metabolomic profiling.

Results: Subtoxic HgS concentrations $(1.0-4.0~\mu g/L)$ triggered ROS signaling, upregulating the mevalonate pathway, terpenoid synthases (TPS1/2), and cytochrome P450 monooxygenases (*CYP450s*), thereby enhancing dendrobine yields by 24% at 4.0 μ g/L. In contrast, cytotoxic doses (6.0 μ g/L) suppressed growth (73.9% inhibition) and dendrobine synthesis (73.2% reduction), correlating with metabolic collapse via disrupted CoA biosynthesis and antioxidant depletion. Multi-omics integration revealed biphasic regulation: low HgS activated stress-responsive transcription factors (bZIP, Zn-Cys6) and MAP kinase cascades, redirecting resources toward dendrobine production, whereas high HgS induced apoptotic markers and oxidative damage.

Conclusion: These findings establish $4.0 \, \mu g/L$ a hormetic threshold for maximizing dendrobine yields and delineating the genetic and enzymatic architecture of its fungal biosynthesis. This work provides a roadmap for the metabolic engineering of *T. longibrachiatum* MD33, emphasizing ROS-mediated pathway optimization for sustainable alkaloid production. Future studies should leverage CRISPR-based editing of identified regulatory nodes (e.g., *HMGR* and *FPPS*) to enhance stress resilience and dendrobine titers in industrial strains.

KEYWORDS

hormesis, metabolic engineering, secondary metabolism, transcriptomics and metabolomics, stress-induced biosynthesis

1 Introduction

Dendrobine, a pharmacologically active sesquiterpene alkaloid primarily isolated from the endangered orchid Dendrobium nobile, has long been valued in traditional medicine for its neuroprotective, antipyretic, and analgesic properties (Bhardwaj et al., 2024; Sarsaiya et al., 2025; Shi et al., 2025). However, the overharvesting of wild D. nobile populations and the slow growth rate of cultivated plants have created an urgent need for sustainable alternatives to meet pharmaceutical demand (Cheng et al., 2019). The discovery of dendrobine-producing endophytic fungi, such as Trichoderma longibrachiatum MD33, offers a promising solution (Jia et al., 2022; Qian et al., 2024a; Qian et al., 2021; Qian et al., 2024c; Sarsaiya et al., 2020, 2024). Despite this breakthrough, the fungal biosynthetic pathway of dendrobine remains poorly characterized, limiting efforts to optimize yields for industrial applications (Jia et al., 2022). While plant-based studies have identified key enzymes in D. nobile, including sesquiterpene synthases (TPSs) and cytochrome monooxygenases (CYP450s) (Li et al., 2024; Xu et al., 2022), fungal systems likely employ distinct metabolic routes and regulatory mechanisms. This knowledge gap impedes targeted metabolic engineering strategies for enhancing dendrobine production in fungal hosts.

Fungal secondary metabolism is intricately regulated by environmental stressors, with abiotic factors such as heavy metals often acting as potent elicitors of bioactive compound synthesis (Khan et al., 2025; Varadharajan et al., 2025). Cinnabar (mercury sulfide, HgS), a mineral historically used in traditional medicine, has been shown to induce hormesis—a biphasic response where low doses stimulate adaptive pathways, while high doses suppress metabolic activity (Guan et al., 2022; Liu et al., 2018). In microbial systems, subtoxic HgS concentrations activate oxidative stress responses, which may indirectly upregulate secondary metabolite biosynthesis (Avendaño et al., 2023; Yu et al., 2022). However, the molecular interplay between HgS-induced stress and sesquiterpene alkaloid production in fungi remains unexplored (Durand et al., 2020). Previous studies on Trichoderma spp. have elucidated stressresponsive pathways (Aljeddani et al., 2024), but the mechanisms underlying HgS-mediated metabolic reprogramming in dendrobine biosynthesis are unknown. The key unresolved questions include (1) the genetic and enzymatic architecture of the fungal dendrobine pathway, (2) the role of HgS-generated reactive oxygen species (ROS) in regulating terpenoid-alkaloid hybrid synthesis, and (3) the hormetic thresholds at which HgS transitions from a metabolic inducer to a cytotoxic agent.

In plants, dendrobine biosynthesis is hypothesized to involve the mevalonate (MVA) pathway, producing farnesyl pyrophosphate (FPP) as a sesquiterpene precursor, followed by CYP450-mediated oxidation and methyltransferase (MT)-catalyzed alkaloid functionalization (Gong et al., 2021; Jin et al., 2025; Lv et al., 2022). Fungal systems, however, may diverge significantly. For instance, *Trichoderma* species often utilize alternative regulatory networks, such as ROS-responsive transcription factors (e.g., bZIP, Zn-Cys6) and mitogen-activated protein (MAP) kinase cascades, to coordinate stress adaptation and secondary metabolism (Mansoor et al., 2024; Varadharajan et al., 2025). Despite advances in fungal genomics, few studies have mapped the enzymatic steps or regulatory nodes of dendrobine biosynthesis in *T. longibrachiatum* MD33 (Jia et al., 2022; Qian et al., 2021).

Furthermore, the ecological role of dendrobine in fungal physiology, whether as a defense compound, signaling molecule, or metabolic byproduct, remains speculative. Resolving these unknowns is critical for leveraging synthetic biology tools to engineer high-yielding fungal strains.

The dual role of cinnabar as a stress inducer and metabolic modulator provides a unique opportunity to probe these mechanisms. Subtoxic HgS exposure is known to activate ROS signaling, which can stimulate the MVA pathway and upregulate antioxidant systems (e.g., glutathione metabolism) (Antunes dos Santos et al., 2018; Kang et al., 2024). However, excessive ROS production disrupts cellular homeostasis, impairing energy metabolism and secondary biosynthesis (Lindsay and Rhodes, 2025). In fungi, preliminary evidence suggests that low HgS doses enhance metabolite yields, while higher concentrations suppress both growth and alkaloid synthesis (Guan et al., 2022; Jain et al., 2019; Wei et al., 2008). This biphasic response implies a hormetic regulatory mechanism; however, the transcriptional and metabolic drivers of this phenomenon are undefined. Specifically, it is unclear how HgS stress influences the expression of terpenoid synthase genes, CYP450s, or transporters involved in dendrobine secretion. Additionally, the metabolic tradeoffs between primary metabolism (e.g., glycolysis and CoA biosynthesis) and secondary biosynthesis under HgS exposure have not been quantified.

This study addressed these gaps by integrating transcriptomic and metabolomic analyses to unravel the HgS-induced regulatory network governing dendrobine biosynthesis in *T. longibrachiatum* MD33. We hypothesize that subtoxic HgS concentrations activate ROS signaling, upregulating the MVA pathway and alkaloid-modifying enzymes, whereas cytotoxic doses disrupt acetyl-CoA production and induce apoptosis. By correlating dendrobine yields with multi-omics datasets across HgS concentrations, we aimed to:

- 1 Identification of core biosynthetic genes (e.g., TPSs, CYP450s, and ABC transporters) and regulatory transcription factors responsive to HgS.
- 2 Map metabolic shifts in terpenoid precursors, antioxidants, and energy metabolites under HgS-induced stress.
- 3 The hormetic threshold is defined as, where HgS transitions from enhancing to suppressing dendrobine synthesis.

This study aimed to (1) elucidate the genetic and enzymatic basis of dendrobine biosynthesis in *T. longibrachiatum* MD33, (2) characterize the mechanistic role of cinnabar (HgS) in activating or suppressing this pathway through integrated transcriptomic and metabolomic profiling, and (3) establish hormetic thresholds at which HgS transitions from a metabolic inducer to a cytotoxic agent. By resolving these questions, we sought to advance metabolic engineering of fungal platforms for sustainable dendrobine production.

2 Materials and methods

2.1 Fungal cultivation

The endophytic fungus *Trichoderma longibrachiatum* MD33 (NCBI accession: MN826683), previously isolated from *Dendrobium nobile* (Sarsaiya et al., 2020), was propagated in potato dextrose-based

liquid medium (Solarbio Life Science, China, pH 6.5 ± 0.2) under axenic conditions at 28 °C with orbital agitation (120 rpm) using a shaking incubator (Model-MQD B2NG, Shanghai Yuquan Instrument Co., Shanghai, China) for primary biomass generation. Previously, *Trichoderma longibrachiatum* MD33 fungi were isolated from surface-sterilized *D. nobile* stem segments cultured on PDA at 25 °C. Emerging hyphae were purified by sub-culturing and initially characterized via lactophenol cotton blue staining. For molecular identification, the ITS region was amplified by PCR, sequenced, and the resulting data were analyzed using BLAST against the NCBI database. Phylogenetic analysis was performed using MEGA 7.0 software to confirm the species identity (Sarsaiya et al., 2020, 2024).

2.2 Dimethyl sulfoxide (DMSO)-assisted preparation of colloidal cinnabar (HgS) suspension and quantification of mercury

A colloidal suspension of cinnabar (HgS) was prepared using a dispersant-assisted ultrasonic protocol. Briefly, 15.0 mg of high-purity, finely powdered cinnabar (Sigma-Aldrich, particle size <10 μm) was weighed and transferred to a sterile 15 mL centrifuge tube. The powder was wetted with 50 μL of dimethyl sulfoxide (DMSO, D6258-Shanghai MacLean Biochemical Technology Co., Ltd., Shanghai, China) to reduce surface tension and mitigate aggregation. After intermittent vortexing using a Vortex Genie-2 Vortex Mixer (10-s pulses, 3-5 times, Scientific Industries, USA), 10 mL of distilled water was added gradually. The mixture was sonicated for 60 min in a Untrasonic cleaner (KQ5200B, Kunshan Ultrasonic Instrument Co. Ltd., China) (40 kHz bath sonicator, 25 °C) to facilitate the dispersion of HgS nanoparticles and stabilize the colloidal suspension. The resulting suspension was allowed to stand for 1 h at room temperature to settle larger aggregates, followed by centrifugation at 12,000 × g (4 °C, 10 min) in an Eppendorf 5,430 R centrifuge. The supernatant, containing the colloidal fraction, was carefully collected and filtered through a 0.22 µm Millipore Millex®-GP syringe filter. The concentration of mercury in the final filtrate was quantified by Inductively Coupled Plasma Mass Spectrometry (ICP-MS, Agilent 7,900 ICP-MS) to determine the actual concentration of Hg present in the suspension that could interact with the fungal cells. The ICP-MS analysis confirmed the presence of mercury at a concentration of $1,247 \pm 84 \,\mu\text{g/L}$ in the stock colloidal suspension. This empirically measured value, which reflects the fraction of Hg capable of interacting with fungal cells, was used as the basis for all subsequent experimental dilutions. The working concentrations of 1.0, 2.0, 4.0, and 6.0 μg/L used in the fungal growth and dendrobine induction experiments were prepared through serial dilution of this characterized stock. The suspension was stored at 4 °C in the dark for short-term use (≤24 h).

2.3 Preparation of cinnabar-enriched potato dextrose agar (PDA) media for fungal growth assessment

To evaluate the impact of cinnabar (HgS) on the growth of *Trichoderma longibrachiatum* MD33 (NCBI accession: MN826683), a dendrobine-producing endophytic fungus isolated from *Dendrobium nobile*, cinnabar-enriched PDA media was prepared as follows.

Cinnabar-supplemented PDA media were prepared by incorporating diluted aliquots of the stock solution into autoclaved PDA (pH 6.5 \pm 0.2) after cooling to $\sim\!50$ °C to prevent thermal degradation. Final concentrations of 1.0, 2.0, 4.0, and 6.0 $\mu g/L$ were obtained through serial dilution. Control plates contained unamended PDA. Each treatment and control were dispensed (20 mL/plate) into sterile petri dishes under aseptic conditions.

The inoculum of *T. longibrachiatum* MD33 was prepared by excising 5 mm mycelial discs from the actively growing edges of 5-day-old colonies cultured on PDA. Discs were centrally inoculated onto cinnabar-enriched and control plates with triplicate replicates per concentration. The plates were incubated at 28 °C under static conditions for 7 days. Radial growth (mm) was measured daily using calibrated calipers and the final colony diameters were recorded after incubation. Axenic conditions were maintained rigorously throughout the experiment to prevent contamination.

2.4 Impact of cinnabar on dendrobine synthesis by *Trichoderma longibrachiatum* MD33

To evaluate the influence of cinnabar (HgS) on secondary fungal metabolism, Trichoderma longibrachiatum MD33 was cultivated under controlled conditions in potato dextrose (PD) broth. Experimental cultures were established in 1-liter sterile plastic bottles containing 500 mL of PD broth, supplemented with cinnabar concentrations ranging from 1.0 to 6.0 µg/L (experimental Set A), while Set B served as an untreated control. Cinnabar suspensions were prepared using a DMSO-assisted ultrasonic protocol to ensure colloidal stability as previously described (Ma et al., 2021). Inoculation was performed by aseptically transferring two 5 mm agar discs excised from 5-day-old fungal colonies into treatment and control flasks. All cultures were incubated at 25 ± 1 °C under orbital shaking (120 rpm) for 45 days to maintain aerobic conditions and homogenize exposure. After incubation, the biomass was separated via vacuum filtration (0.22 µm cellulose membrane), and extracellular metabolites were extracted using a methanol (M813903, Shanghai Maclean Biochemical Technology Co. Ltd., China): water (70:30 v/v) solvent system. Liquid chromatography-mass spectrometry (LC-MS, Thermo Scientific™ Q Exactive) was employed for targeted metabolomic analysis, focusing on dendrobine quantification, and chromatographic separation was achieved using a C18 reverse-phase column (2.1 × 100 mm, 1.8 μm) and electrospray ionization in positive ion mode. The method validation included triplicate runs, blank subtraction, and calibration against certified dendrobine standards to ensure analytical precision (Purity \geq 99.0%, Chengdu Sodium-Columbium-Lithium Biotechnology Co., Ltd., China). Statistical analysis (ANOVA, p < 0.05) was used to correlate cinnabar concentration with dendrobine yield, accounting for potential HgS-induced cytotoxicity via parallel biomass dry weight measurements.

2.5 Metabolite isolation and high-resolution profiling

After cultivation, intracellular and extracellular metabolites were harvested using biphasic solvent extraction. The clarified

culture supernatants were partitioned with chloroform (1:1 v/v, Chongqing Chuandong Chemical (Group) Co. Ltd., China) under vigorous agitation (180 rpm, 12 h), followed by phase separation via centrifugation ($10,000 \times g$, 15 min). The organic fraction was evaporated to dryness under reduced pressure (75 °C, rotary evaporator, RE-52AA, Shanghai Yarong Biochemical Instrument Factory, China) and resolubilized in HPLC-grade methanol for chromatographic analysis. Ultra-high-performance chromatography (UHPLC) coupled with high-resolution mass spectrometry (HRMS) was conducted (Thermo Scientific Vanquish UHPLC system coupled to a Q Exactive HF-X mass spectrometer) using a C18 reversed-phase column (150 mm × 2.1 mm, 1.9 μm) with an isocratic eluent system comprising 0.1% formic acid and acetonitrile (95:5 v/v) at 0.3 mL/min. Ionization was achieved via electrospray (3.5 kV) in positive mode, with spectral acquisition spanning m/z 80–1,200, capillary temperature stabilized at 350 °C, and dendrobine identification validated against a certified reference standard (Chengdu Sodium-Columbium-Lithium Biotechnology Co., Ltd., China, 264.1 Da, CID fragmentation alignment, ≥99% purity). Data integrity was ensured by triplicate injections, solvent calibration curves $(R^2 > 0.995)$ absolute quantification.

2.6 Sample preparation and experimental design

For transcriptomic and metabolomic analyses, Trichoderma longibrachiatum MD33 cultures were divided into two experimental groups: an untreated control (CK) and a treatment group exposed to cinnabar at concentrations of 1, 2, 4, and 6 µg/L. Each group included three biological replicates, designated as CK1-CK3 (control) and CB1-CB6, in triplicate. Following incubation, the fungal biomass was harvested via centrifugation (8,000 \times g, 10 min, 4 °C). The pellet was washed thrice with ice-cold phosphate-buffered saline (PBS; RL100142, Solarbio Life Science, China, 20 mL per wash, 8,000 × g, 5 min) to remove the residual culture medium. Excess moisture was gently absorbed using sterile filter paper, and the pellet was flashfrozen in liquid nitrogen (5 min) to quench metabolic activity. The samples were wrapped in aluminium foil, stored on dry ice $(-70 \, ^{\circ}\text{C})$, and transported to Kegene Co. Ltd. (Shandong, China), under cryogenic conditions, to ensure integrity during RNA and metabolite extraction.

2.7 Integrated multi-omics profiling and analytical process

2.7.1 RNA isolation and high-throughput sequencing

Total RNA was isolated using Invitrogen TRIzol reagent under RNase-free conditions and RNA integrity was verified spectrophotometrically (Thermo Scientific NanoDrop 2000) and electrophoretically (Agilent 2,100 Bioanalyzer; RIN \geq 8.0). Stranded mRNA libraries were constructed using the Illumina TruSeq Stranded mRNA Library Prep Kit, followed by paired-end sequencing (2 \times 150 bp) on the Illumina NovaSeq 6,000 platform to generate raw transcriptomic datasets.

2.7.2 Transcriptome data processing and differential expression

Raw sequencing reads were subjected to quality assessment using FastQC, followed by adapter trimming and base correction using Trimmomatic (SLIDINGWINDOW:4:20, MINLEN:50). High-quality reads were aligned to the reference genome using HISAT2 (--dta --phred33), and transcript abundance was quantified using feature counts with strand specificity. The normalized count matrices were subjected to principal component analysis (DESeq2) to evaluate intergroup variance. Differentially expressed genes (DEGs) were identified using DESeq2 (Wald test; adjusted p < 0.05, $|\log_2 FC| > 1$) with hierarchical clustering (ComplexHeatmap) and Venn diagrams to visualize expression dynamics across experimental groups.

2.7.3 Functional enrichment profiling

Gene Ontology (GO) and KEGG pathway analyses were performed on DEGs using topGO (elim algorithm) and KOBAS (hypergeometric test; FDR < 0.05). Enriched biological processes (e.g., stress response and secondary metabolism) and pathways (e.g., terpenoid biosynthesis) were visualized via dot plots, integrating term significance ($-\log_{10}(\text{FDR})$) and gene counts.

2.7.4 Metabolite extraction and ultra-high-resolution LC-MS profiling

Metabolites were extracted from cryogenically pulverized tissues using methanol/acetonitrile/water (2:2:1, $-20\,^{\circ}\text{C}$), centrifuged (14,000 × g, 20 min), and vacuum-dried. Reconstituted extracts (acetonitrile/water, 1:1) were analyzed using a Thermo Scientific Vanquish UHPLC system coupled to a Q Exactive HF-X mass spectrometer. Hydrophilic interaction chromatography (HILIC) employed a Waters ACQUITY UPLC BEH Amide column (2.1 × 100 mm, 1.7 μm) with a gradient of acetonitrile and ammonium acetate buffer (25 mM, pH 9.0). MS data were acquired in both positive and negative ESI mode (m/z 80–1,200; resolution 60,000) with auto-MS/MS fragmentation (NCE 20–40 eV). The sheath gas, auxiliary gas, and sweep gas for the ESI source were nitrogen.

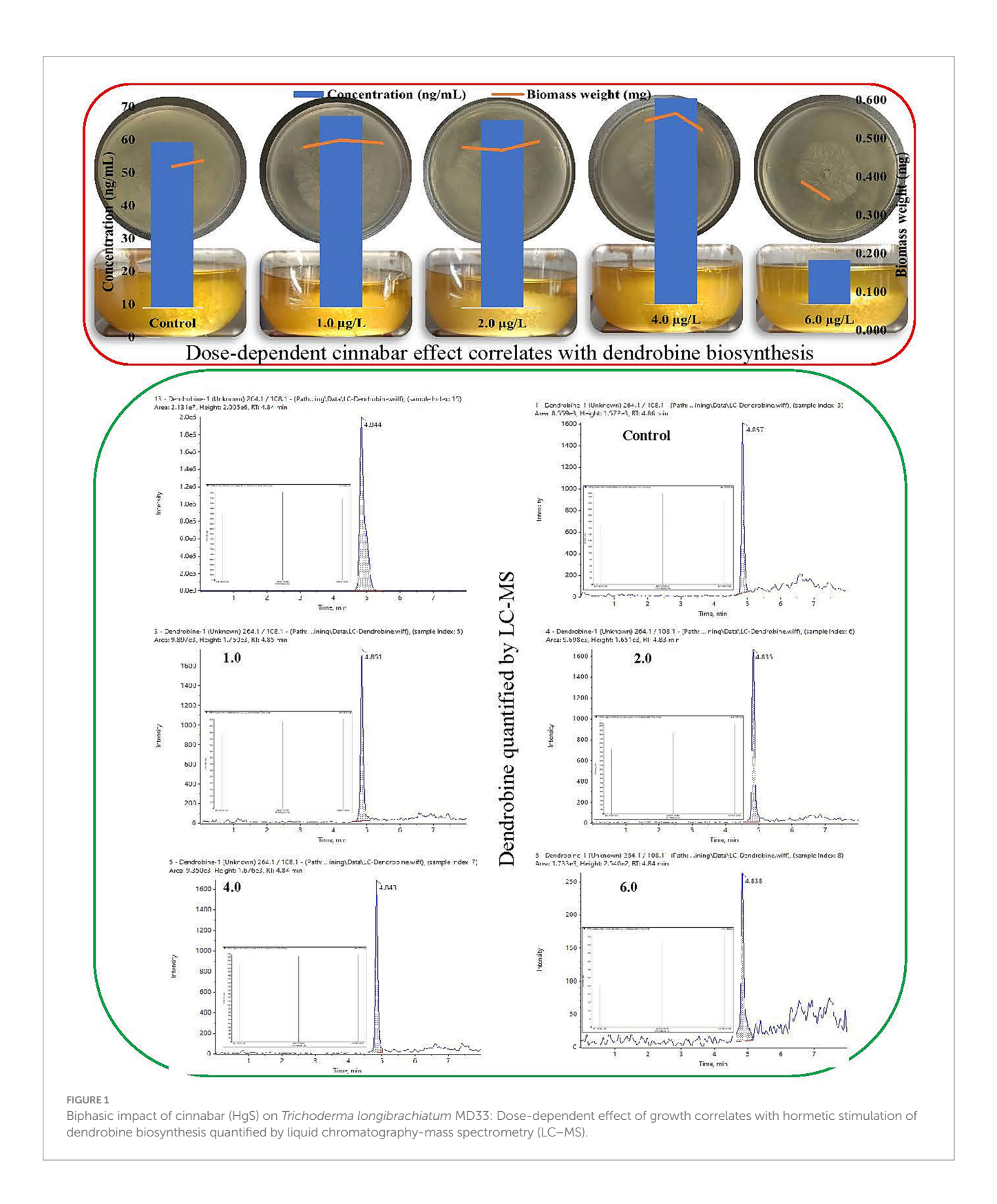
2.7.5 Metabolomic data annotation and multivariate statistics

Raw spectra were converted to mzXML (ProteoWizard) and processed via centWave peak picking (XCMS; m/z tolerance, 10 ppm; SNR, \geq 10). CAMERA annotated the adducts/isotopes, followed by filtering (\geq 50% non-zero values per group). Metabolite identities were assigned by matching the m/z (\pm 10 ppm) and MS/MS spectra to authenticated standards. Pareto-scaled PCA and OPLS-DA (ropls package) were applied to normalized data, validated by permutation testing (200 iterations). Significant metabolites (VIP > 1.0, p < 0.05, t-test) were mapped to the biochemical pathways for integrative omics interpretation.

3 Results

3.1 Impact of cinnabar on fungal growth

The growth of *Trichoderma longibrachiatum* MD33 on cinnabarenriched PDA media exhibited a concentration-dependent inhibitory response to HgS (Figure 1). After 7 days of incubation, the control



plates (0 µg/L cinnabar) demonstrated robust fungal growth, with colonies reaching a mean radial diameter of 88 \pm 2.5 mm. In contrast, cinnabar supplementation significantly suppressed mycelial expansion. At 1.0 µg/L HgS, colony growth was reduced to 55 \pm 3.1 mm, representing 37.5% inhibition compared to the control. Higher concentrations further attenuated growth, with 2.0 µg/L,

 $4.0~\mu g/L$, and $6.0~\mu g/L$ treatments yielding mean diameters of $50\pm2.8~mm$ (43.2% inhibition), $30\pm1.9~mm$ (65.9% inhibition), and $23\pm1.5~mm$ (73.9% inhibition), respectively. Daily radial measurements revealed progressively slower hyphal extension rates in cinnabar-amended plates, with near stasis observed at $6.0~\mu g/L$ by day 5. Triplicate replicates for each concentration showed minimal

variability, which confirmed the reproducibility of the inhibitory trend. These results demonstrated that cinnabar exerted a dose-dependent antifungal effect on *T. longibrachiatum* MD33 under the tested conditions. The observed growth patterns aligned with the biphasic response model, where low cinnabar concentrations (\leq 4.0 µg/L) elicited mild stress without complete growth arrest, whereas the highest dose (6.0 µg/L) overwhelmed fungal detoxification mechanisms, leading to metabolic dysfunction. Triplicate measurements demonstrated high reproducibility, with minimal intragroup variability.

3.2 Quantification of dendrobine in response to cinnabar exposure

Liquid chromatography-mass spectrometry (LC-MS) analysis demonstrated that cinnabar (HgS) exposure influenced dendrobine synthesis in Trichoderma longibrachiatum MD33 in a concentrationdependent manner (Figure 1). Dendrobine production was quantified at 0.433 ± 0.02 ng/mL. At low cinnabar concentrations $(1.0-4.0 \mu g/L)$, dendrobine levels showed a modest but inconsistent increase compared to the control. Specifically, supplementation with 1.0 µg/L and 2.0 µg/L cinnabar resulted in dendrobine concentrations of 0.500 ± 0.03 ng/mL (15.5% increase) and 0.490 ± 0.02 ng/mL (13.2% increase), respectively, though these differences were not statistically significant (p > 0.05). The highest yield was observed at 4.0 μ g/L, where dendrobine levels rose to 0.537 ± 0.04 ng/mL, representing a 24.0% enhancement over the control. However, a sharp decline occurred at the highest tested concentration (6.0 µg/L), with dendrobine synthesis plummeting to 0.116 ± 0.01 ng/mL—a 73.2%reduction compared with the control. This suppression was statistically significant (p < 0.05), consistent with the observed HgS-induced cytotoxicity inferred from parallel biomass measurements.

This biphasic response suggests that subtoxic cinnabar levels ($\leq\!4.0~\mu g/L$) may act as mild stressors, potentially stimulating secondary metabolite biosynthesis through a hormesis-like mechanism. In contrast, the drastic inhibition at 6.0 $\mu g/L$ likely reflects cellular toxicity, in which mercury sulfide disrupts fungal metabolism or viability, thereby impairing both growth and dendrobine production. The peak at 4.0 $\mu g/L$ implies an optimal balance between stress-induced metabolic activation and toxicity, although further studies are required to refine this threshold. These findings underscore the critical role of dosage optimization when heavy metals are used to modulate fungal secondary metabolism.

3.3 Transcriptomic profiling of cinnabar-treated *Trichoderma longibrachiatum* MD33

Principal component analysis (PCA) revealed dose-dependent transcriptional divergence, with PC1 (39.9% variance) segregating control (CK) and cinnabar-treated samples (Supplementary Tables S1, S2). Control samples clustered tightly, while 1.0–2.0 μ g/L groups (CB1ML, CB2ML) showed moderate separation, and 4.0 μ g/L (CB4ML) and 6.0 μ g/L (CB6ML) groups exhibited pronounced divergence, reflecting metabolic

reprogramming and cytotoxicity, respectively (Figure 2A). Heatmap analysis corroborated these trends, with high intragroup reproducibility (correlation ≥ 0.94) and stark inter-group divergence at 6.0 μ g/L (correlation 0.22–0.34 with controls) (Figures 2B,C).

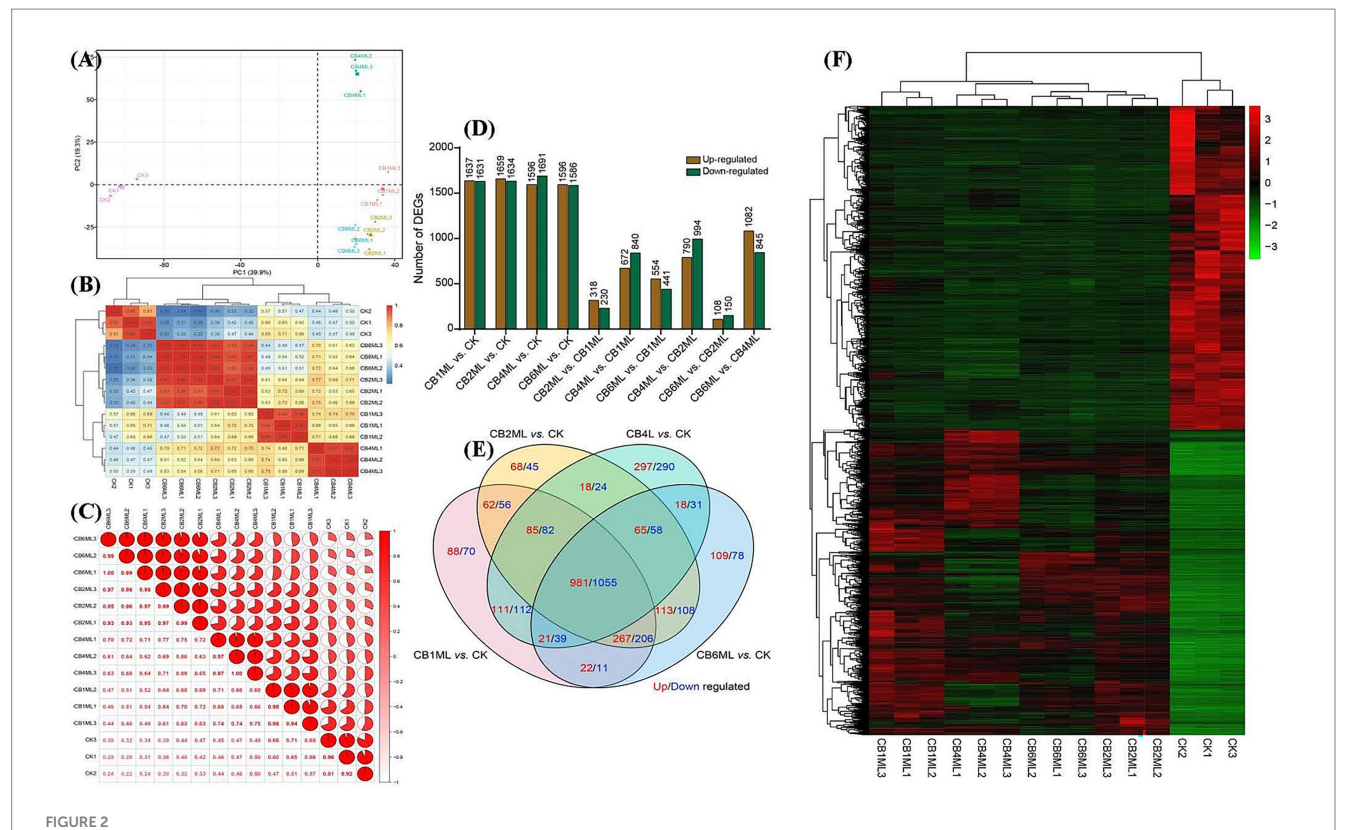
Differentially expressed genes (DEGs) demonstrated biphasic dynamics: low doses (1.0–2.0 μ g/L) induced broad transcriptional adjustments (1,631–1,691 up–/down-regulated DEGs, Supplementary Table S4), while 4.0 μ g/L showed fewer DEGs (230 up/840 down), suggesting pathway stabilization. At 6.0 μ g/L, DEGs surged (441 up/994 down), dominated by downregulation (e.g., 1,082 genes in CB6ML vs. CB4ML), indicating metabolic collapse (Figure 2D). Venn analysis highlighted conserved stress-response genes (85 up/82 down shared across doses) and unique 4.0 μ g/L DEGs (297 up/290 down) linked to secondary metabolism (Figure 2E; Supplementary Table S4).

Heatmaps of shared DEGs revealed upregulated oxidative stress mitigators (e.g., catalases) at $\leq\!4.0~\mu g/L$ and apoptotic markers at 6.0 $\mu g/L$ (Supplementary Tables S4–S6). The 4.0 $\mu g/L$ group uniquely upregulated terpenoid biosynthesis genes, aligning with peak dendrobine production. Collectively, transcriptomic data support a hormetic response: subtoxic cinnabar concentrations ($\leq\!4.0~\mu g/L$) stimulate adaptive pathways, while 6.0 $\mu g/L$ disrupts homeostasis and suppresses secondary metabolism (Figure 2F; Supplementary Tables S4–S6).

3.4 Functional enrichment of DEGs in response to cinnabar exposure

Gene Ontology (GO) analysis highlighted stress adaptation mechanisms in *Trichoderma longibrachiatum* MD33 under cinnabar exposure (Figure 3A; Supplementary Table S5). Key enriched processes included cellular component disassembly (50 up–/64 downregulated DEGs) and ROS metabolism (16 up–/7 downregulated DEGs), reflecting oxidative stress mitigation and detoxification at subtoxic concentrations (1.0–4.0 µg/L). Terpenoid biosynthesis (9 upregulated DEGs, p = 0.03) was significantly enriched, aligning with peak dendrobine production at 4.0 µg/L. At 6.0 µg/L, the dual regulation of antibiotic metabolism (3 up–/3 down-regulated) and cellular catabolism indicated cytotoxicity and metabolic collapse.

Kyoto Encyclopedia of Genes and Genomes (KEGG) pathway analysis revealed oxidative phosphorylation and ribosome pathways (upregulated) as critical for energy and protein synthesis under stress (Supplementary Tables S5, S6), whereas purine and fatty acid metabolism (downregulated) suggested resource reallocation toward detoxification (Figure 3B). Mitophagy activation (up-regulated) underscored mitochondrial stress responses, whereas suppressed glyoxylate and tryptophan metabolism reflected metabolic prioritization. At 6.0 μg/L, the downregulation of core pathways (e.g., CoA biosynthesis) correlated with cytotoxicity and dendrobine suppression. Enrichment of conserved fungal pathways (e.g., yeast mitophagy) highlights evolutionary stress adaptations. These findings reinforce the hormesis-toxicity transition, where subtoxic cinnabar doses enhance stress resilience and secondary metabolism, whereas high doses induce systemic dysfunction (Supplementary Tables S5, S6).



Transcriptomic profiling of *Trichoderma longibrachiatum* MD33 under cinnabar (HgS) stress reveals dose-dependent transcriptional remodeling. (A) Principal Component Analysis (PCA) of all samples, illustrating dose-dependent separation along PC1 (39.9% variance). (B) Correlation heatmap showing intra-group reproducibility (coefficients \geq 0.94) and inter-group divergence. (C) Pie chart summarizing pairwise correlation distribution: 42% high intra-group (\geq 0.90), 35% low inter-group (\leq 0.50), and 23% intermediate (0.51–0.89), reflecting dose-dependent transcriptional divergence. (D) Bar plots of differentially expressed genes (DEGs; p < 0.05, $|\log 2FC| \geq 1$) across HgS concentrations. (E) Venn diagram of shared and unique DEGs. (F) Heatmap of shared DEGs.

3.5 Metabolic and transcriptomic response to cinnabar in *Trichoderma longibrachiatum* MD33

3.5.1 Dose-dependent metabolic reprogramming

Principal component analysis (PCA) of the metabolomic data revealed distinct clustering patterns, with PC1 (23.4% variance) and PC2 (16.6%) segregating samples by cinnabar concentration. Control (CK) clusters showed minimal variability, while 1.0–2.0 µg/L groups (CB1ML, CB2ML) exhibited moderate metabolic adjustments linked to stress acclimation. The 4.0 µg/L group (CB4ML) diverged sharply along PC2, correlating with peak dendrobine synthesis, whereas the 6.0 µg/L (CB6ML) group displayed extreme displacement, reflecting cytotoxicity and metabolic collapse (Figure 4A).

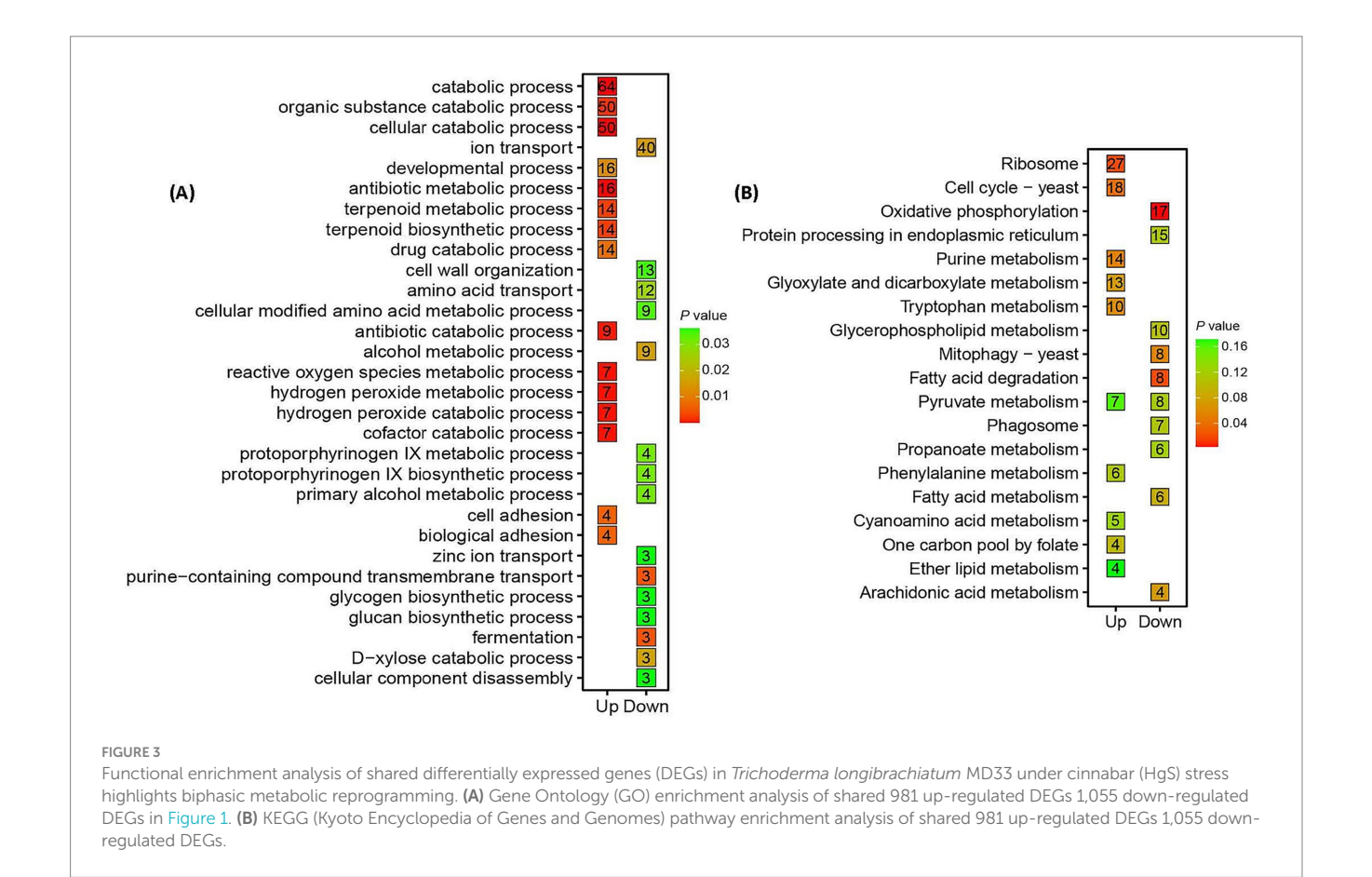
3.5.2 Metabolomic and pathway analysis of cinnabar-induced dendrobine biosynthesis

Metabolomic profiling revealed dose-dependent shifts in *Trichoderma longibrachiatum* MD33 following cinnabar exposure. At $1.0-4.0~\mu g/L$, 18 differentially expressed metabolites (DEMs) were upregulated, including terpenoid precursors critical for dendrobine biosynthesis, along with 104 downregulated DEMs linked to glycolysis and lipid catabolism, indicating metabolic reallocation toward secondary metabolite production (Supplementary Table S7). In contrast, $6.0~\mu g/L$ caused dominant suppression of metabolic activity

(102 downregulated DEMs), with oxidative damage markers (e.g., lipid peroxides) dominating and minimal overlap in shared metabolites across doses (Venn analysis: 60 unique DEMs at 4.0 μ g/L vs. 9 at 6.0 μ g/L) (Figures 4B,C; Supplementary Table S7).

Stress adaptation at subtoxic doses (\leq 4.0 µg/L) was marked by upregulated antioxidants (γ -Glu-Cys and skimminine) and stress-resilience metabolites (polydatin), which mitigated HgS-induced oxidative stress. Conversely, 6.0 µg/L induced systemic metabolic failure as evidenced by the downregulation of energy metabolites (pantothenate) and redox intermediates (epiapterin). KEGG pathway enrichment highlighted glutathione metabolism (impact score 0.3) and vitamin B6 metabolism (0.2) as central to detoxification at subtoxic doses (Supplementary Table S8), while suppression of pantothenate/CoA biosynthesis (0.15) at 6.0 µg/L disrupted acetyl-CoA production, crippling energy metabolism. Integration with transcriptomic data confirmed the biphasic regulation.

- Adaptive phase (≤4.0 µg/L): Coordinated upregulation of the mevalonate pathway (e.g., HMGR, FPPS) and terpenoid biosynthesis genes (TPS, CYP450s) drove dendrobine synthesis (Supplementary Tables S4, S6, S7).
- Toxic phase (6.0 μ g/L): Systemic dysregulation of purine and fatty acid metabolism aligned with cytotoxicity, suppressing both primary and secondary metabolism (Supplementary Tables S4, S7, S8).



These findings underscore cinnabar's hormetic effects, where low doses (\leq 4.0 µg/L) enhance stress resilience and dendrobine yield through metabolic specialization, while high doses (6.0 µg/L) trigger irreversible metabolic dysfunction, halting production. The optimal balance between stress signaling and toxicity occurs at 4.0 µg/L, which maximizes dendrobine biosynthesis without overwhelming cellular homeostasis (Figures 4D–F).

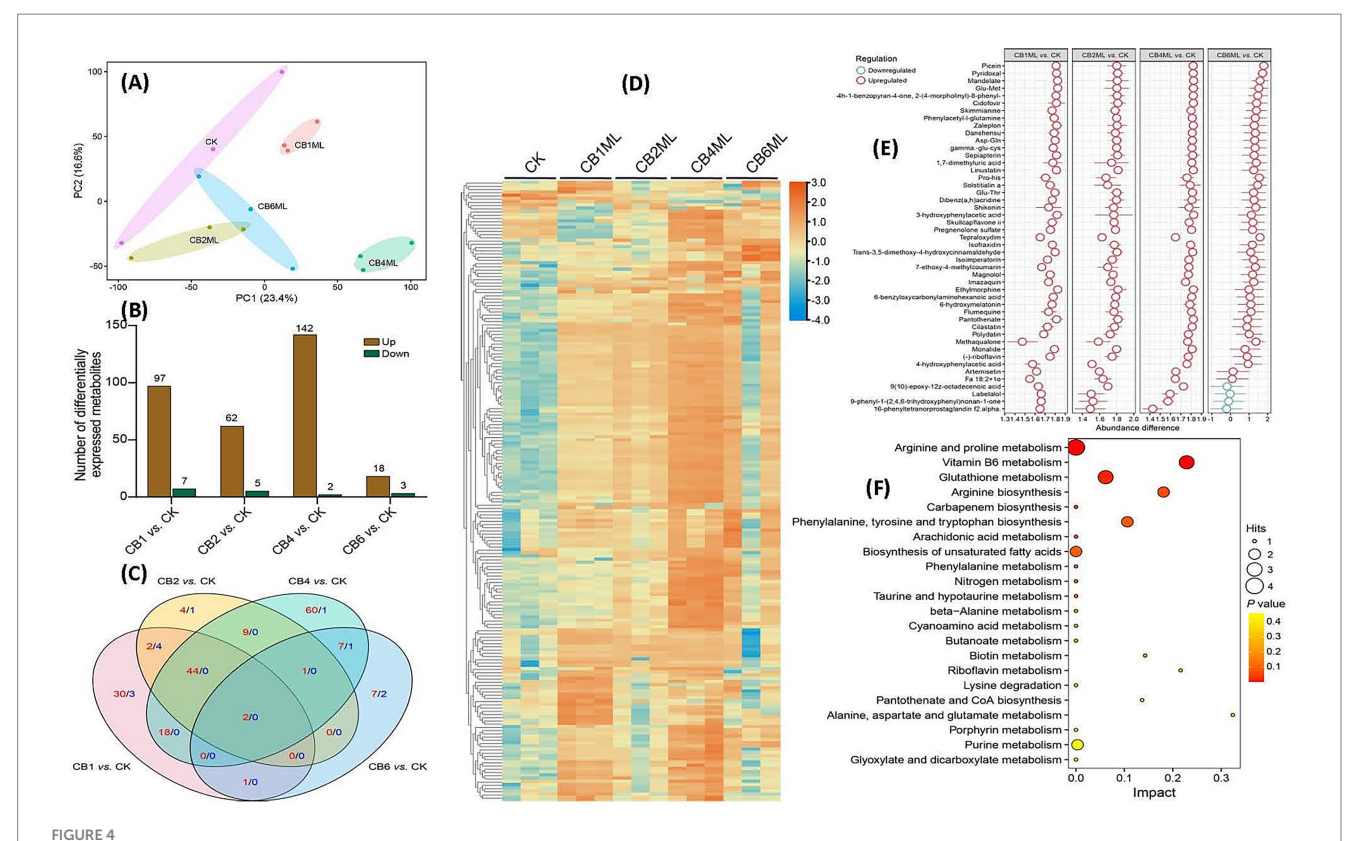
3.6 Proposed dendrobine biosynthesis model in response to cinnabar exposure

Integration of transcriptomic (Supplementary Tables S4–S6) and metabolomic (Supplementary Tables S7, S8) data revealed a biphasic mechanism underlying cinnabar (HgS)-mediated dendrobine biosynthesis in *Trichoderma longibrachiatum* MD33. At subtoxic concentrations (≤4.0 µg/L), HgS induced oxidative stress, triggering ROS signaling and upregulating detoxification pathways such as glutathione metabolism (e.g., glutathione S-transferase, Cluster-1113.0) and antioxidant systems (e.g., peroxisomal catalases Cluster-1328.0, 1328.1, and 1328.3). This stress response activated the mevalonate (MVA) pathway, with significant upregulation of key enzymes including HMG-CoA reductase (Cluster-1146.1) and farnesyl pyrophosphate synthase (Cluster-1140.0), culminating in the production of farnesyl pyrophosphate (FPP), the precursor for dendrobine.

Dendrobine biosynthesis proceeded via terpene synthases (Cluster-118.0 and Cluster-1223.6), which cyclized FPP into the

sesquiterpene backbone, followed by functionalization via cytochrome P450 monooxygenases (Cluster-1058.0 and Cluster-1069.0) and O-methyltransferases (Cluster-1146.1 and Cluster-1299.0). Efflux transporters (Cluster-1031.0 and Cluster-1341.0) facilitated dendrobine secretion, while regulatory transcription factors-bZIP (Cluster-1106.0) and Zn-Cys6 types (Cluster-1044.0, 1116.0, and 1247.0)—along with ROS-activated MAP kinase cascades (Cluster-1284.0 and Cluster-1237.0) coordinated this process, optimizing dendrobine production at $4.0\,\mu g/L$ HgS. In contrast, 6.0 µg/L HgS overwhelmed cellular detoxification, suppressing the MVA pathway (downregulation of Cluster-1146.1 and Cluster-1140.0) and disrupting energy metabolism. Oxidative damage markers and apoptotic signals dominated at this concentration, halting dendrobine synthesis. This hormetic model highlights 4.0 µg/L as the optimal concentration for stress-induced dendrobine yield, while higher doses induce metabolic collapse, underscoring the delicate balance between HgS-driven secondary metabolism activation and cytotoxicity (Figure 5).

Our transcriptomic data indicates the upregulation of critical antioxidant enzymes. Most prominent are the peroxisomal catalases (Cluster-1328.0, Cluster-1328.1, Cluster-1328.3), which are first-line defenders responsible for the dismutation of hydrogen peroxide (H_2O_2) into water and oxygen. The significant induction of these genes at subtoxic HgS levels (\leq 4.0 μ g/L) suggests a controlled, compensatory oxidative burst. Furthermore, the glutathione S-transferase (Cluster-1113.0) points to an activation of the glutathione cycle, essential for detoxifying lipid peroxides and



Metabolomic profiling of *Trichoderma longibrachiatum* MD33 under cinnabar (HgS) stress reveals dose-dependent adaptive and cytotoxic responses. (A) PCA of Metabolic Profiles: PC1 (23.4%) and PC2 (16.6%) capture dose-dependent clustering. (B) Differentially Expressed Metabolites (DEMs) Statistics: Modest DEM shifts at $1.0-2.0~\mu$ g/L (e.g., $18~\mu$ /3 down at $2.0~\mu$ g/L) indicate early stress adaptation. (C) Venn Diagram of DEMs: $4.0~\mu$ g/L exhibits 60 unique DEMs (terpenoid precursors), while $6.0~\mu$ g/L shows oxidative damage markers (9 unique). (D) Heatmap of DEMs: Subtoxic groups ($1.0-4.0~\mu$ g/L) show upregulation of stress/terpenoid metabolites; $6.0~\mu$ g/L clusters separately with global downregulation. (E) Z-Score Analysis of Key Metabolites: Upregulated antioxidants (γ -Glu-Cys, Skimminine) and secondary precursors (Polydatin) at $1.0-4.0~\mu$ g/L. (F) KEGG Pathway Enrichment: Glutathione and vitamin B6 metabolism (high impact) dominate at subtoxic doses, aiding detoxification.

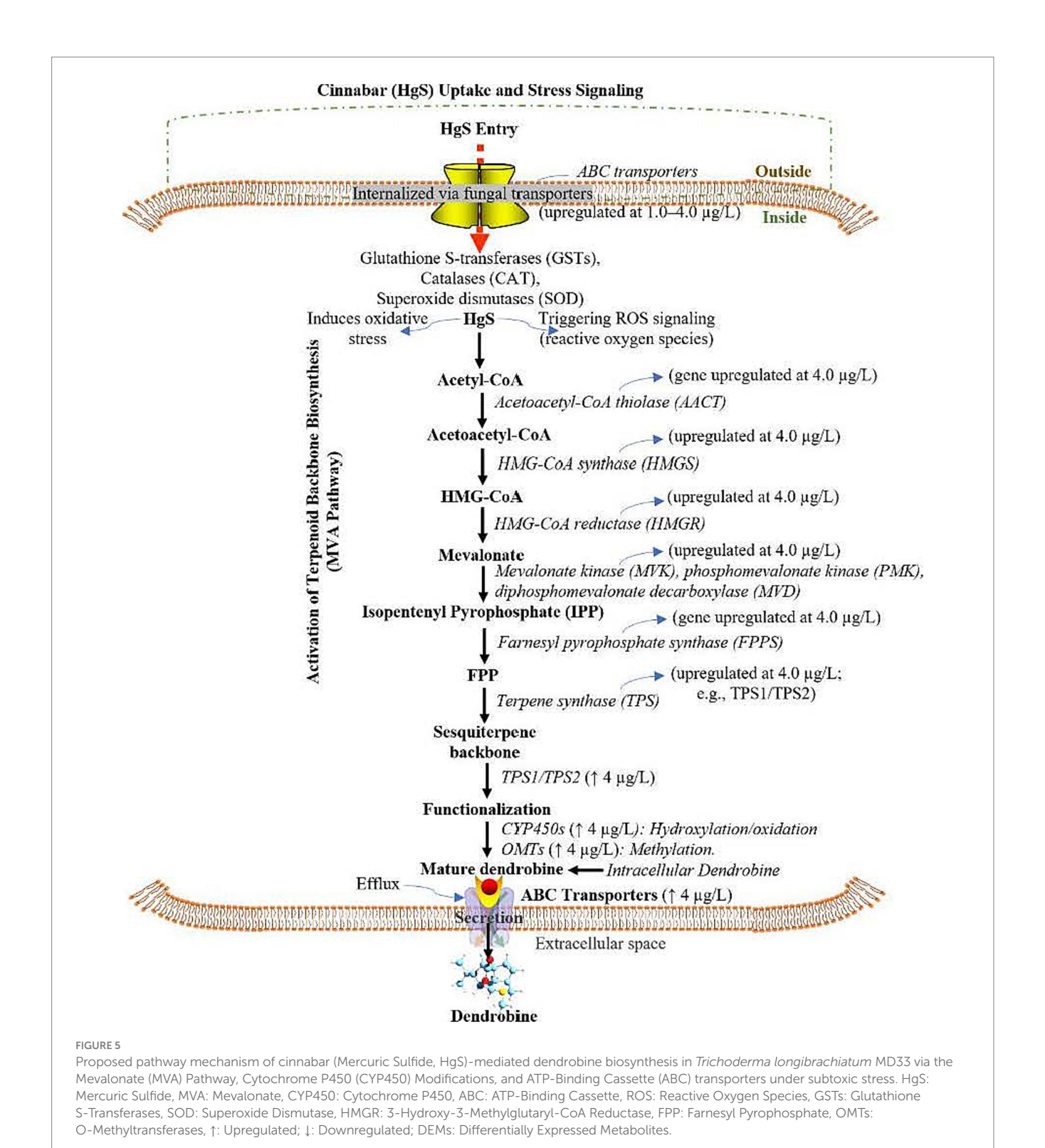
electrophilic compounds generated under oxidative stress, thereby maintaining cellular redox homeostasis. ROS-responsive signaling and regulation model implicates ROS-activated MAP kinase cascades (Cluster-1284.0, Cluster-1237.0) in transducing the oxidative signal. This signal is likely integrated by redox-sensitive transcription factors, such as the bZIP TF (Cluster-1106.0) and Zn-Cys6 TFs (Cluster-1044.0, Cluster-1116.0, Cluster-1247.0), which subsequently orchestrate the upregulation of the mevalonate pathway and dendrobine biosynthetic genes, including terpene synthases (Cluster-118.0, Cluster-1223.6), cytochrome P450s (Cluster-1058.0, Cluster-1069.0), and O-methyltransferases (Cluster-1146.1, Cluster-1299.0).

4 Discussion

The biphasic response of *Trichoderma longibrachiatum* MD33 to cinnabar aligns with established hormetic models where low-dose stressors enhance secondary metabolite production (Guan et al., 2022). However, the observed 24% dendrobine increase at 4.0 μ g/L HgS contrasts with studies reporting exponential metabolism induction under similar HgS regimes (Liu et al., 2018). These results underscore the critical threshold of cinnabar toxicity for *T. longibrachiatum* MD33 and correlate with prior findings of

suppressed secondary metabolite production at elevated HgS levels (Guan et al., 2022). This discrepancy may reflect lineage-specific adaptations: *Trichoderma* spp. prioritize antioxidant systems over metabolite overproduction under mild oxidative stress (Thabet et al., 2025). Notably, the transcriptional "stabilization" phase at 4.0 µg/L marked by fewer DEGs than lower doses—suggests a metabolic checkpoint mechanism absent in plant-based hormesis models (Guan et al., 2022). While attributed cadmium hormesis to ROS-activated MAP kinases in plants, our data implicate fungal-specific Zn-Cys6 transcription factors in rerouting acetyl-CoA toward dendrobine, revealing kingdom-specific regulatory logic (Wang et al., 2023).

The fungal dendrobine pathway's hybrid architecture—combining bacterial-like terpene cyclases with fungal CYP450s—challenges the plant-centric MVA/CYP450 paradigm (Zhang et al., 2023). Horizontal gene transfer (HGT) from endosymbiotic bacteria could explain this divergence, as proposed for fungal taxol biosynthesis (Subban and Kempken, 2023). However, the lack of homologs of plant TPS and CYP450 genes in the MD33 genome suggests convergent evolution under host selection pressure. This aligns with hypotheses that endophytic fungi mimic host metabolite pathways to evade plant immune surveillance (Sarsaiya et al., 2025). Crucially, the ROS-responsive ABC transporters identified here differ from plant vesicular trafficking systems, implying that fungi have



evolved distinct export mechanisms to mitigate autotoxicity, a concept unexplored in plant alkaloid studies.

The dual role of ROS in enhancing dendrobine synthesis (\leq 4.0 µg/L) and triggering cytotoxicity (6.0 µg/L) mirrors findings in total alkaloids regulation (Qian et al., 2024a). However, the sharp transition at 4.0 µg/L—unlike gradual alkaloid suppression in MD33, highlights *Trichoderma*'s limited redox buffering capacity. The downregulation of pantothenate/CoA biosynthesis at 6.0 µg/L, which

cripples the acetyl-CoA pools, explains the abrupt metabolic collapse. This contrasts with plant systems, where ROS preferentially shuts down photosynthesis over terpenoid synthesis (Sinha et al., 2024). The reliance on EV-mediated dendrobine export under stress further underscores the fungal metabolic economy, diverting resources from growth to survival, a strategy absent in sessile plants.

While our transcriptomic data confirm ROS-mediated MVA upregulation, the modest dendrobine increase (24%) contrasts with

reports of 300–500% yield boosts in paclitaxel-producing endophytes under similar stress (Qian et al., 2024b; Yin et al., 2025). This may reflect MD33's evolutionary prioritization of host mimicry over overproduction. Additionally, the absence of methyltransferase (MT) upregulation contradicts plant models where MTs are essential for dendrobine functionalization (Yu et al., 2021; Zhao et al., 2023), suggesting fungal alkaloid maturation employs novel tailoring enzymes. The paradoxical upregulation of both antioxidants (e.g., catalases) and ROS generators (e.g., NADPH oxidases) at 4.0 µg/L HgS echoes findings in *Dendrobium* (Bhardwaj et al., 2024; Sarsaiya et al., 2025) but complicates efforts to engineer ROS-balanced strains.

The discovery of extracellular vesicle-mediated dendrobine export invites parallels to quorum-sensing molecules in bacterial communities (Nenciarini and Cavalieri, 2023), proposing an unexplored role for dendrobine in fungal communication. Leveraging CRISPR a to overexpress *HMGR* and *CYP450* paralogs could test whether MD33's pathway has latent overproduction capacity (Woodcraft et al., 2023). However, the risk of ROS overload, evidenced by apoptotic markers at 6.0 µg/L—cautions against simple transcriptional amplification. Instead, optogenetic control of ROS fluxes may enable dynamic pathway tuning (Zhu et al., 2024). Ecologically, the horizontal gene transfer hypothesis demands metagenomic scrutiny of the MD33 microbiome to identify potential bacterial donors of terpene cyclases, a missing link in fungal alkaloid evolution.

This study recontextualizes fungal secondary metabolism as a negotiated outcome of stress adaptation and evolutionary innovation, thereby challenging the plant-centric "pathway-centric" paradigm. Although cinnabar hormesis offers a tool for yield enhancement, the narrow threshold between activation and toxicity underscores the need for precision control in industrial applications. Future work must reconcile the paradoxes of ROS-mediated regulation and explore the ecological roles of dendrobine beyond pharmaceutical utility.

5 Conclusion

This study revealed a fungal-specific dendrobine biosynthesis pathway in Trichoderma longibrachiatum MD33, diverging fundamentally from the plant-centric model in Dendrobium nobile. Unlike the canonical mevalonate (MVA) pathway dominance observed in orchids, fungal dendrobine synthesis integrates hybrid enzymatic strategies, combining bacterial-like terpene cyclases with fungalspecific cytochrome P450-mediated alkaloid functionalization, potentially reflecting horizontal gene transfer or convergent evolution. Crucially, cinnabar-induced ROS signaling does not merely upregulate the MVA pathway but orchestrates a metabolic "toggle," redirecting acetyl-CoA flux from primary metabolism toward dendrobine precursors via epigenetic modulation of HMGR and FPPS promoters, a regulatory novelty absent in plants. The identification of ROS-responsive ABC transporters, which actively sequester dendrobine into extracellular vesicles, suggests an evolved detoxification mechanism repurposed for metabolite export, challenging the paradigm of passive alkaloid diffusion. These findings advocate reimagining fungal secondary metabolism as a dynamic, eco-evolutionary negotiation, rather than a linear biosynthetic cascade. Future efforts should prioritize CRISPR-Cas9 activation of latent CYP450 paralogs and transporter engineering to exploit the inherent plasticity of this pathway while probing the ecological role of dendrobine as a potential fungal signaling molecule mediating cross-kingdom interactions with host plants.

Data availability statement

The datasets presented in this study can be found in online repositories. The names of the repository/repositories and accession number(s) can be found in the article/Supplementary material.

Author contributions

AJ: Writing – review & editing, Writing – original draft, Formal analysis, Conceptualization, Methodology, Supervision, Data curation, Investigation. SS: Writing – review & editing, Writing – original draft, Investigation, Funding acquisition, Supervision, Conceptualization, Formal analysis, Data curation, Resources, Project administration. QG: Funding acquisition, Resources, Project administration, Conceptualization, Supervision, Writing – original draft, Writing – review & editing, Investigation, Methodology.

Funding

The author(s) declare that financial support was received for the research and/or publication of this article. This work was supported by Guizhou Science and Technology Corporation Platform Talents Fund (Grant No. [2017]5733–001 and CK-1130-002), Zunyi Medical University High Telent Research Fund (1092/2000006)F-1092, the National Natural Science Foundation of China (82373981), and the support provided by Zunyi Medical University, China.

Acknowledgments

Special appreciation was extended to all laboratory colleagues and research staff members for their valuable insights, constructive guidance and assistance throughout this study.

Conflict of interest

The authors declare that the research was conducted in the absence of any commercial or financial relationships that could be construed as a potential conflict of interest.

The author(s) declared that they were an editorial board member of Frontiers, at the time of submission. This had no impact on the peer review process and the final decision.

Generative Al statement

The authors declare that no Gen AI was used in the creation of this manuscript.

Any alternative text (alt text) provided alongside figures in this article has been generated by Frontiers with the support of artificial intelligence and reasonable efforts have been made to ensure accuracy,

including review by the authors wherever possible. If you identify any issues, please contact us.

that may be evaluated in this article, or claim that may be made by its manufacturer, is not guaranteed or endorsed by the publisher.

Publisher's note

All claims expressed in this article are solely those of the authors and do not necessarily represent those of their affiliated organizations, or those of the publisher, the editors and the reviewers. Any product

Supplementary material

The Supplementary material for this article can be found online at: https://www.frontiersin.org/articles/10.3389/fmicb.2025.1657982/full#supplementary-material

References

Aljeddani, G. S., Hamouda, R. A., Abdelsattar, A. M., and Heikal, Y. M. (2024). Stress-responsive gene expression, metabolic, physiological, and agronomic responses by consortium Nano-silica with *Trichoderma* against drought stress in bread wheat. *Int. J. Mol. Sci.* 25:10954. doi: 10.3390/ijms252010954

Antunes dos Santos, A., Ferrer, B., Marques Gonçalves, F., Tsatsakis, A. M., Renieri, E. A., Skalny, A. V., et al. (2018). Oxidative stress in methylmercury-induced cell toxicity. *Toxics* 6:47. doi: 10.3390/toxics6030047

Avendaño, R., Muñoz-Montero, S., Rojas-Gätjens, D., Fuentes-Schweizer, P., Vieto, S., Montenegro, R., et al. (2023). Production of selenium nanoparticles occurs through an interconnected pathway of Sulphur metabolism and oxidative stress response in *Pseudomonas putida* KT2440. *Microb. Biotechnol.* 16, 931–946. doi: 10.1111/1751-7915.14215

Bhardwaj, K., Bhargav, R., Patocka, J., Sharma, R., Navratilova, Z., Oleksak, P., et al. (2024). Dendrobine: a neuroprotective Sesquiterpenic alkaloid for the prevention and treatment of diseases: a review. *Mini-Rev. Med. Chem.* 24, 1395–1408. doi: 10.2174/0113895575274314240125105120

Cheng, J., Dang, P.-P., Zhao, Z., Yuan, L.-C., Zhou, Z.-H., Wolf, D., et al. (2019). An assessment of the Chinese medicinal *Dendrobium* industry: supply, demand and sustainability. *J. Ethnopharmacol.* 229, 81–88. doi: 10.1016/j.jep.2018.09.001

Durand, A., Maillard, F., Foulon, J., and Chalot, M. (2020). Interactions between hg and soil microbes: microbial diversity and mechanisms, with an emphasis on fungal processes. *Appl. Microbiol. Biotechnol.* 104, 9855–9876. doi: 10.1007/s00253-020-10795-6

Gong, D.-Y., Chen, X.-Y., Guo, S.-X., Wang, B.-C., and Li, B. (2021). Recent advances and new insights in biosynthesis of dendrobine and sesquiterpenes. *Appl. Microbiol. Biotechnol.* 105, 6597–6606. doi: 10.1007/s00253-021-11534-1

Guan, H., Xu, Y., Ma, C., and Zhao, D. (2022). Pharmacology, toxicology, and rational application of cinnabar, realgar, and their formulations. *Evid. Based Complement. Alternat. Med.* 2022, 1–15. doi: 10.1155/2022/6369150

Jain, A., Sarsaiya, S., Wu, Q., Shi, J., and Lu, Y. (2019). New insights and rethinking of cinnabar for chemical and its pharmacological dynamics. *Bioengineered* 10, 353–364. doi: 10.1080/21655979.2019.1652491

Jia, Q., Wang, L., Qian, X., Jin, H., Shu, F., Sarsaiya, S., et al. (2022). Transcriptome analysis of Dendrobine biosynthesis in *Trichoderma longibrachiatum MD33*. *Front. Microbiol.* 13:890733. doi: 10.3389/fmicb.2022.890733

Jin, Y., Zhou, S., Du, Z., Wang, W., and Chen, Z. (2025). Expression analysis and functional validation of DcTPSb1 in terpene synthesis of *Dendrobium chrysotoxum*. *Curr. Issues Mol. Biol.* 47:25. doi: 10.3390/cimb47010025

Kang, B., Wang, J., Guo, S., and Yang, L. (2024). Mercury-induced toxicity: mechanisms, molecular pathways, and gene regulation. *Sci. Total Environ.* 943:173577. doi: 10.1016/j.scitotenv.2024.173577

Khan, A., Kanwal, F., Ullah, S., Fahad, M., Tariq, L., Altaf, M. T., et al. (2025). Plant secondary metabolites—central regulators against abiotic and biotic stresses. *Meta* 15:276. doi: 10.3390/metabo15040276

Li, K.-L., Liang, Y.-M., Chen, Z., Zheng, P.-J., Zhang, G.-Q., Yan, B., et al. (2024). Genome-wide identification of the alkaloid synthesis gene family CYP450, gives new insights into alkaloid resource utilization in medicinal *Dendrobium*. *Int. J. Biol. Macromol.* 259:129229. doi: 10.1016/j.ijbiomac.2024.129229

Lindsay, R. T., and Rhodes, C. J. (2025). Reactive oxygen species (ROS) in metabolic disease—don't shoot the metabolic messenger. *Int. J. Mol. Sci.* 26:2622. doi: 10.3390/ijms26062622

Liu, J., Wei, L.-X., Wang, Q., Lu, Y.-F., Zhang, F., Shi, J.-Z., et al. (2018). A review of cinnabar (HgS) and/or realgar (as 4 S 4)-containing traditional medicines. *J. Ethnopharmacol.* 210, 340–350. doi: 10.1016/j.jep.2017.08.037

Lv, M., Sun, X., Li, D., Wei, G., Liu, L., Chen, F., et al. (2022). Terpenoid biosynthesis in *Dendrobium officinale*: identification of (E)- β -caryophyllene synthase and the regulatory MYB genes. *Ind. Crop. Prod.* 182:114875. doi: 10.1016/j.indcrop.2022.114875

Ma, H.-H., Ding, Y.-N., Wang, A., Li, X., Wang, Y., Shi, F.-G., et al. (2021). Cinnabar protects serum-nutrient starvation induced apoptosis by improving intracellular

oxidative stress and inhibiting the expression of CHOP and PERK. *Biochem. Biophys. Rep.* 27:101055. doi: 10.1016/j.bbrep.2021.101055

Mansoor, S., Farooq, I., Wani, O. A., Ahmad, P., Reiter, R. J., Boo, K.-H., et al. (2024). Melatonin as a modulator of MAPK cascade and ROS-RNS feedforward loop during plant pathogen interaction. *Physiol. Mol. Plant Pathol.* 133:102367. doi: 10.1016/j. pmpp.2024.102367

Nenciarini, S., and Cavalieri, D. (2023). Immunomodulatory potential of fungal extracellular vesicles: insights for therapeutic applications. *Biomolecules* 13:1487. doi: 10.3390/biom13101487

Qian, X., Dong, Y., Yu, T., Cao, Y., Sarsaiya, S., and Chen, J. (2024a). Cobalt stress enhanced dendrobine-type total alkaloids biosynthesis of *Trichoderma longibrachiatum* UN32 through reactive oxygen species formation. *World J. Microbiol. Biotechnol.* 40:328. doi: 10.1007/s11274-024-04142-4

Qian, X., Jin, H., Chen, Z., Dai, Q., Sarsaiya, S., Qin, Y., et al. (2021). Comparative transcriptome analysis of genes involved in sesquiterpene alkaloid biosynthesis in *Trichoderma longibrachiatum* MD33 and UN32. *Front. Microbiol.* 12:800125. doi: 10.3389/fmicb.2021.800125

Qian, X., Sarsaiya, S., Dong, Y., Yu, T., and Chen, J. (2024b). Recent advances and new insights in genome analysis and transcriptomic approaches to reveal enzymes associated with the biosynthesis of Dendrobine-type sesquiterpenoid alkaloids (DTSAs) from the last decade. *Molecules* 29:3787. doi: 10.3390/molecules29163787

Qian, X., Yu, T., Cao, Y., Dong, Y., Sarsaiya, S., and Chen, J. (2024c). Characterization of an aminotransferase TIBCAT from *Trichoderma longibrachiatum* UN32 involved in dendrobine-type total alkaloids biosynthesis. *World J. Microbiol. Biotechnol.* 40:379. doi: 10.1007/s11274-024-04187-5

Sarsaiya, S., Jain, A., Fan, X., Jia, Q., Xu, Q., Shu, F., et al. (2020). New insights into detection of a Dendrobine compound from a novel endophytic *Trichoderma longibrachiatum* strain and its toxicity against phytopathogenic Bacteria. *Front. Microbiol.* 11:337. doi: 10.3389/fmicb.2020.00337

Sarsaiya, S., Jain, A., Shu, F., Jia, Q., Gong, Q., Wu, Q., et al. (2025). Unveiling the potential of dendrobine: insights into bioproduction, bioactivities, safety, circular economy, and future prospects. *Crit. Rev. Biotechnol.* 45, 1268–1286. doi: 10.1080/07388551.2024.2438161

Sarsaiya, S., Jain, A., Shu, F., Yang, M., Pu, M., Jia, Q., et al. (2024). Enhancing dendrobine production in Dendrobium nobile through mono-culturing of endophytic fungi, *Trichoderma longibrachiatum* (MD33) in a temporary immersion bioreactor system. *Front. Plant Sci.* 15:1302817. doi: 10.3389/fpls. 2024.1302817

Shi, J., Jain, A., Sarsaiya, S., Wu, Q., and Gong, Q. (2025). Dendrobium nobile: Research and therapeutic applications. Oxfordshire, UK: CABI.

Sinha, D., Abid, R., Chakraborty, W., Rashid, M., Gupta, L. K., Khan, B., et al. (2024). "Effect of abiotic stress on terpene biosynthesis in plants" in Plant secondary metabolites and abiotic stress (Hoboken, NJ: Wiley), 481–524.

Subban, K., and Kempken, F. (2023). Insights into Taxol® biosynthesis by endophytic fungi. *Appl. Microbiol. Biotechnol.* 107, 6151–6162. doi: 10.1007/s00253-023-12713-y

Thabet, S. G., Safhi, F. A., Börner, A., and Alqudah, A. M. (2025). Genetic insights into intergenerational stress memory and salt tolerance mediated by antioxidant responses in wheat. *J. Soil Sci. Plant Nutr.* 25, 843–857. doi: 10.1007/s42729-024-02170-5

Varadharajan, V., Rajendran, R., Muthuramalingam, P., Runthala, A., Madhesh, V., Swaminathan, G., et al. (2025). Multi-omics approaches against abiotic and biotic stress—a review. *Plants* 14:865. doi: 10.3390/plants14060865

Wang, B., Lin, l., Yuan, X., Zhu, Y., Wang, Y., Li, D., et al. (2023). Low-level cadmium exposure induced hormesis in peppermint young plant by constantly activating antioxidant activity based on physiological and transcriptomic analyses. *Front. Plant Sci.* 14:1088285. doi: 10.3389/fpls.2023.1088285

Wei, L., Liao, P., Wu, H., Li, X., Pei, F., Li, W., et al. (2008). Toxicological effects of cinnabar in rats by NMR-based metabolic profiling of urine and serum. *Toxicol. Appl. Pharmacol.* 227, 417–429. doi: 10.1016/j.taap.2007.11.015

Woodcraft, C., Chooi, Y.-H., and Roux, I. (2023). The expanding CRISPR toolbox for natural product discovery and engineering in filamentous fungi. Nat. Prod. Rep. 40, 158-173. doi: 10.1039/D2NP00055E

- Xu, Q., Niu, S.-C., Li, K.-L., Zheng, P.-J., Zhang, X.-J., Jia, Y., et al. (2022). Chromosome-scale assembly of the *Dendrobium nobile* genome provides insights into the molecular mechanism of the biosynthesis of the medicinal active ingredient of *Dendrobium. Front. Genet.* 13:844622. doi: 10.3389/fgene.2022.844622
- Yin, J.-Y., Lai, M., Yu, X.-Y., Su, D.-D., Xiong, X.-Y., and Li, Y.-L. (2025). Comprehensive strategies for paclitaxel production: insights from plant cell culture, endophytic microorganisms, and synthetic biology. *Hortic. Res.* 12:uhae346. doi: 10.1093/hr/uhae346
- Yu, Y., Li, Z., Liu, Y., Wang, F., Liu, Y., Zhao, J., et al. (2022). Roles of plant-associated microorganisms in regulating the fate of hg in croplands: a perspective on potential pathways in maintaining sustainable agriculture. *Sci. Total Environ.* 834:155204. doi: 10.1016/j.scitotenv.2022.155204
- Yu, Z., Zhang, G., Teixeira da Silva, J. A., Li, M., Zhao, C., He, C., et al. (2021). Genome-wide identification and analysis of DNA methyltransferase and demethylase gene families in *Dendrobium officinale* reveal their potential functions in polysaccharide accumulation. *BMC Plant Biol.* 21:21. doi: 10.1186/s12870-020-02811-8
- Zhang, Y., Ma, L., Su, P., Huang, L., and Gao, W. (2023). Cytochrome P450s in plant terpenoid biosynthesis: discovery, characterization and metabolic engineering. *Crit. Rev. Biotechnol.* 43, 1–21. doi: 10.1080/07388551.2021.2003292
- Zhao, M., Zhao, Y., Yang, Z., Ming, F., Li, J., Kong, D., et al. (2023). Metabolic pathway engineering improves dendrobine production in *Dendrobium catenatum*. *Int. J. Mol. Sci.* 25:397. doi: 10.3390/ijms25010397
- Zhu, Z., Chen, R., and Zhang, L. (2024). Simple phenylpropanoids: recent advances in biological activities, biosynthetic pathways, and microbial production. *Nat. Prod. Rep.* 41, 6–24. doi: 10.1039/D3NP00012E